9.5 NUMERICAL SIMULATION OF THE INTERACTION BETWEEN THE DRYLINE AND HORIZONTAL CONVECTIVE ROLLS

Steven E. Peckham,*[1] Robert B. Wilhelmson,[1] Louis J. Wicker,[2] and Conrad L. Ziegler[2]

[1]Department of Atmospheric Sciences, University of Illinois at Urbana-Champaign, Urbana, Illinois
[2]National Severe Storms Laboratory, Norman, Oklahoma

1. INTRODUCTION

Over the past decade, fine-scale observational studies have revealed that atmospheric boundaries (e.g., sea-breezes, convergence zones, drylines) can possess a large amount of along-line variation (Wilson et al. 1992, Atkins et al. 1995, Atkins et al. 1998). These studies focused on the relationship between these along-line variations to the presence of horizontal convective rolls (HCRs) within the boundary layer (Etling and Brown 1993, Brown 1980). The results suggest that, besides producing along-line undulations, enhanced ascent occurs where HCR updrafts intersect the boundaries. Further, convective clouds form in the region of enhanced ascent.

With the increase in computational resources over the past decade, researchers using numerical models are beginning to investigate the interaction between convective rolls and atmospheric boundaries. For example, Dailey and Fovell (1999) demonstrated that high-resolution (500-m) simulations of the sea breeze could reproduce many of the observed phenomena (e.g., sea-breeze boundary, HCRs). These simulations also demonstrate how the interaction between HCRs and boundaries plays an important role in the formation and evolution of convective clouds along the sea breeze.

Numerical studies of drylines interacting with boundary layer HCRs have been recently reported in the literature (e.g., Ziegler et al. 1997, Peckham 1999). These simulations use a horizontal resolution that is marginally capable of resolving HCRs (i.e., 1-km), but produce many of the observed phenomena (e.g., a dryline, HCRs, deep moist convection). Interestingly, these simulations produce HCRs with aspect ratios much larger than those explained by classic linear theory. One possible explanation for the large aspect ratio is the nonlinear interaction between individual HCRs and/or gravity waves in the free troposphere. Another possible cause of the large aspect ratios is the limiting of convective roll scales that can occur in nested grid numerical simulations where the inner grid is too small.

With the advances in computational power, it is now possible to conduct single-grid high-resolution simulations of the dryline environment in order to investigate daytime morphology of HCRs near a developing dryline, the HCR-dryline interactions and subsequent convective cloud formation. Expanding upon previous results (Peckham and Wicker 2000, Peckham 1999), this investigation examines the formation of HCRs within the daytime dryline environment using a high horizontal resolution (1000 m) numerical simulation. Some of the goals of this study are:

- to increase the understanding of the along-line variability of the dryline in relation to the HCR/dryline interaction.
- to increase the understanding of how the HCRs interact with the dryline to aid in the formation of convective storms.

*Corresponding author address: Steven E. Peckham, NOAA/FSL, R/FS1, DSRC, 325 Broadway, Boulder, CO 80305
e-mail: steven.peckham@noaa.gov.

2. METHODOLOGY

The COllaborative Model for Multiscale Atmospheric Simulation (COMMAS) is used in this study (Peckham 1999, Wicker and Wilhelmson 1995). COMMAS includes a generalized terrain-following coordinate transformation (Gal-Chen and Sommerville 1975), parameterizations for surface radiation for a cloudy atmosphere (Benjamin 1986) and land surface processes (Deardorff 1972, 1978). A 1.5-order sub-grid scale turbulence parameterization (Deardorff 1980) is used with the vertical mixing length within the unstable boundary layer following Sun and Chang (1986).

A 12-hour simulation is performed on a 600 km x 60 km numerical grid having 1-km horizontal resolution and centered at 100° W longitude and 34.5° N latitude. The domain extends vertically to 18 km with a vertical mesh interval smoothly stretching from 50 m at the lowest grid point to approximately 500 m at the domain top. Open lateral boundary conditions (Klemp and Wilhelmson 1978) are applied on the eastern and western edges of the domain, and periodic boundary conditions are employed at the northern and southern domain edges. Numerical damping is used to eliminate wave reflection from the rigid domain top.

Rather than attempt a simulation with detailed terrain information, the terrain elevation is confined to changes in the x-direction and is expressed analytically using a hyperbolic tangent function (Peckham 1999). The use of an analytical expression permits the close approximation of the actual terrain without introducing the high-frequency variations associated with realistic topography.

The initial thermodynamic profile (Fig. 1), derived from 1200 UTC observational data obtained during the Cooperative Oklahoma Profiler Studies–1991 (COPS-91) field program, varies in the east-west direction (Hane et al. 1993, Peckham 1999). For the

experiments, the zonal vertical wind shear is .004 s^{-1} below 4.5 km MSL and is incrementally relaxed to zero vertical shear above 6 km MSL (Fig. 2). The initial v wind component is assumed to be uniformly 6 m s^{-1} and in geostrophic balance. The low-level let is initialized as an elliptical region of super-geostrophic southerly flow with a maximum wind speed increase of 5 m s^{-1}.

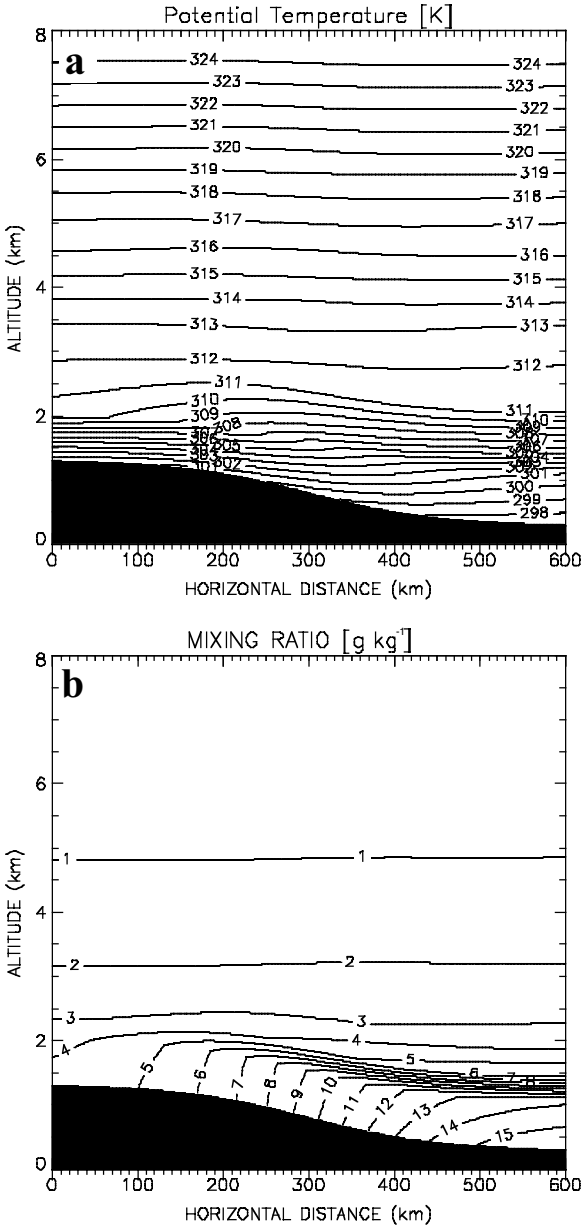

Fig. 1. Cross-section plot along y=30 km of the initial virtual potential temperature (a) and mixing ratio (b). The contour interval is 1 K and 1 g kg^{-1} respectively. The black shading depicts the sloping terrain used in the simulation.

The initial volumetric soil moisture (hereafter soil moisture) and fractional vegetation coverage (hereafter vegetation) are also specified analytically (Fig. 3). The eastern most section of the domain is moist and predominantly covered in vegetation while the western domain is initially relatively dry with relatively sparse vegetation. At x=600 km (eastern boundary) the surface soil moisture is initially set at 0.3, the deep soil moisture at 0.36 and vegetation at 0.6. At x=0 km (western boundary) the surface soil moisture is 0.75, the deep soil moisture is 0.26, and the vegetation is 0.3. Further, random fluctuations, in x and y, of 0.02 times the initial value are applied to the soil moisture and vegetation field. The surface roughness, vegetation albedo and soil type are assumed constant across the entire domain and are set to 0.1, 0.21, and sandy loam respectively.

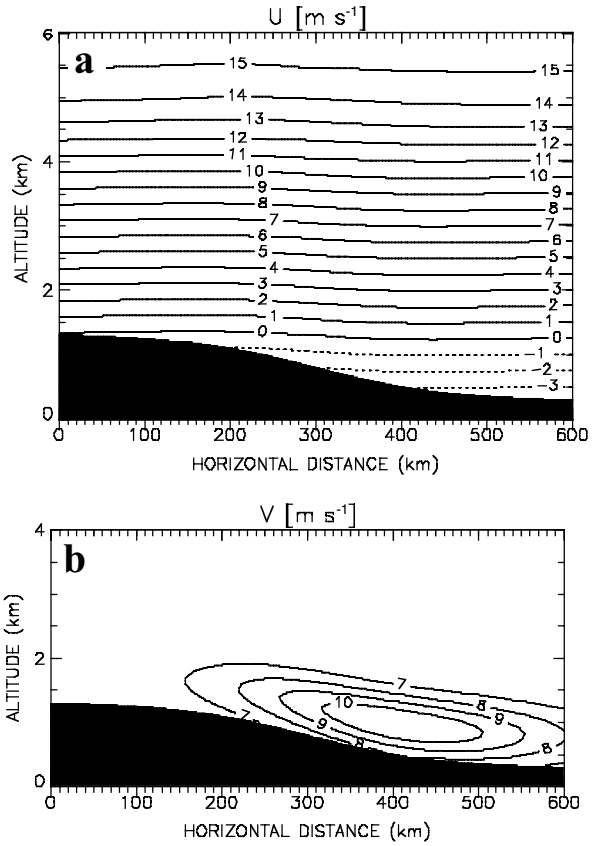

Fig. 2. Cross-section plot along y=30 km of the initial vertical profile for the u (a) and v (b) wind components. The dash lines represent negative values. The black shading depicts the sloping terrain used in the simulation.

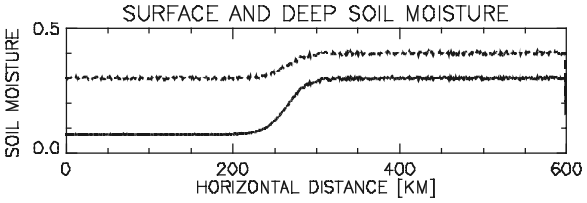

Fig. 3. Initial profile along y=30 km for the surface volumetric soil moisture and deep soil volumetric soil moisture (dashed line). The random fluctuations in both fields are not uniform in the y-direction.

3. EXPERIMENTAL RESULTS

Relatively weak to moderate bands of HCRs develop within the simulated convective boundary layer (CBL) around 3.5 hours. The rolls initially develop in two separate regions, near the eastern domain boundary and along the sloping terrain at the domain's center. The rolls are oriented in the direction of the local mean CBL wind. The roll aspect ratio (ratio of distance between consecutive roll updrafts to updraft depth) ranges from approximately 15 near the eastern boundary to approximately 20 at the domain center. The range in aspect ratios appears related to the deeper CBL near the eastern boundary. Over the next hour the CBL deepens as the surface is heated and vigorous horizontal convective rolls develop across the simulation domain (Fig. 4). The CBL top is roughly 1km to 1.5 km AGL with roll updraft spacing estimated to be 5 to 6 km apart (aspect ratios range from approximately 4 to 6).

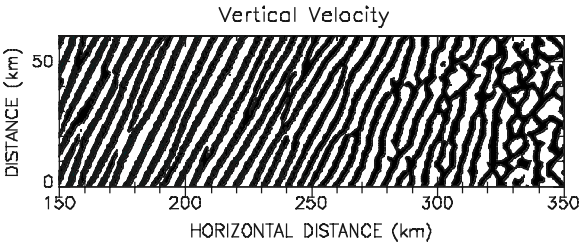

Fig. 4. Horizontal plot of the vertical velocity along the fifth vertical grid level (approximately 500 m AGL). The shaded (white) regions depict locations of ascending (descending) motion.

The simulated HCRs are similar to observed convective rolls in that they develop during the morning hours in an unstably stratified boundary layer, and are orientated in the direction of the mean boundary layer flow (Weckwerth et al. 1999). Also, the aspect ratio of the simulated rolls is in close agreement with observations and theory (Brown 1980; Etling and Brown 1993; Asai 1970, 1972).

Eight hours into the simulation, the HCR bands have evolved into a random open cellular structure (Fig. 5). This evolution from linear bands to cellular structure has been reported before in the literature (e.g., Grossman 1982, Weckwerth 1997). Suggested regions include the combination of HCRs, increased boundary layer instability and interaction between HCRs and gravity waves in the overlying stable atmosphere (Weckwerth 1999, Redelsperger and Clark 1990). In addition, a strong west to east horizontal moisture gradient, or dryline, has developed at the surface near x=251 km. The horizontal mixing ratio gradient in this region is approximately 0.4 g kg^{-1} km^{-1}.

Over the next hour, the dryline makes little eastward progression. However, east-west undulations along the dryline boundary are located along the dryline, at approximately every 10 to 15 km. These undulations propagate northward along the dryline boundary at roughly 5 m s^{-1}. In addition, the undulations appear to be coincident with intersection locations of HCRs from the eastern and western boundary. Here the dryline bows westward (eastward) at the intersection of the western HCR updrafts (downdrafts) with the dryline boundary. This result is in close agreement with Atkins et al. (1998) who hypothesized that the interaction of the western HCRs with the dryline is responsible for creating a considerable amount of along-line variations. Further, the along-line undulations are similar to the undulations observed along the sea breeze and reproduced in

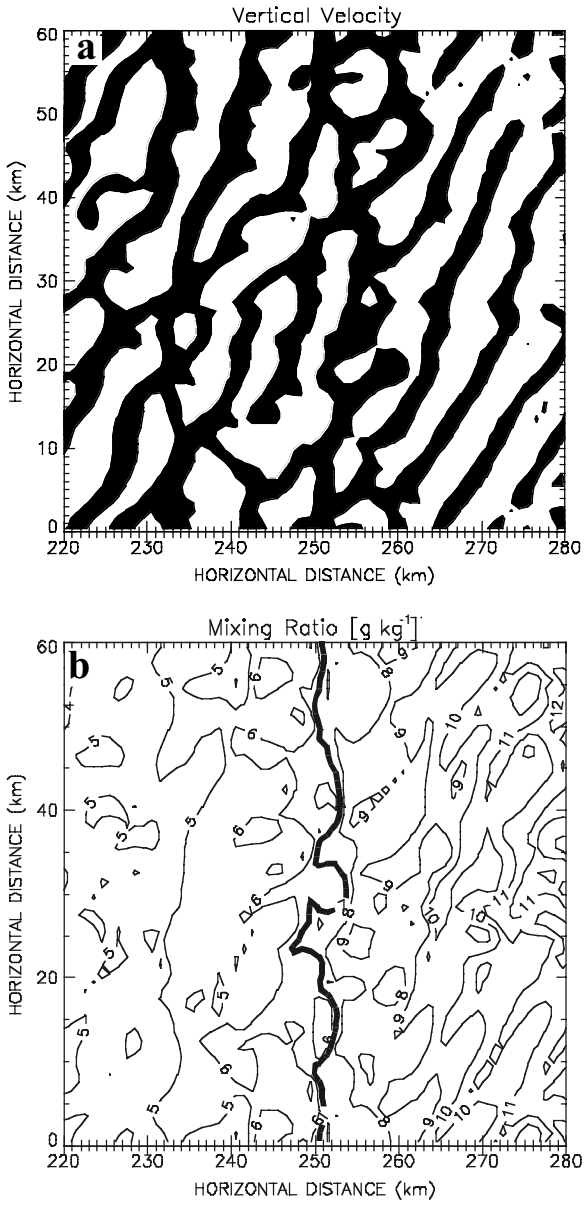

Fig. 5. (a) Horizontal plot of the vertical velocity along the tenth vertical grid level (approximately 1 km AGL) at 8 hours into the simulation. The shaded (white) regions represent locations of ascending (descending) motion. (b) Horizontal plot of the surface-level mixing ratio at 8 hours into the simulation. The contour interval is 1 g kg^{-1} respectively with the 7 g kg^{-1} isohume (approximate dryline location) bolded.

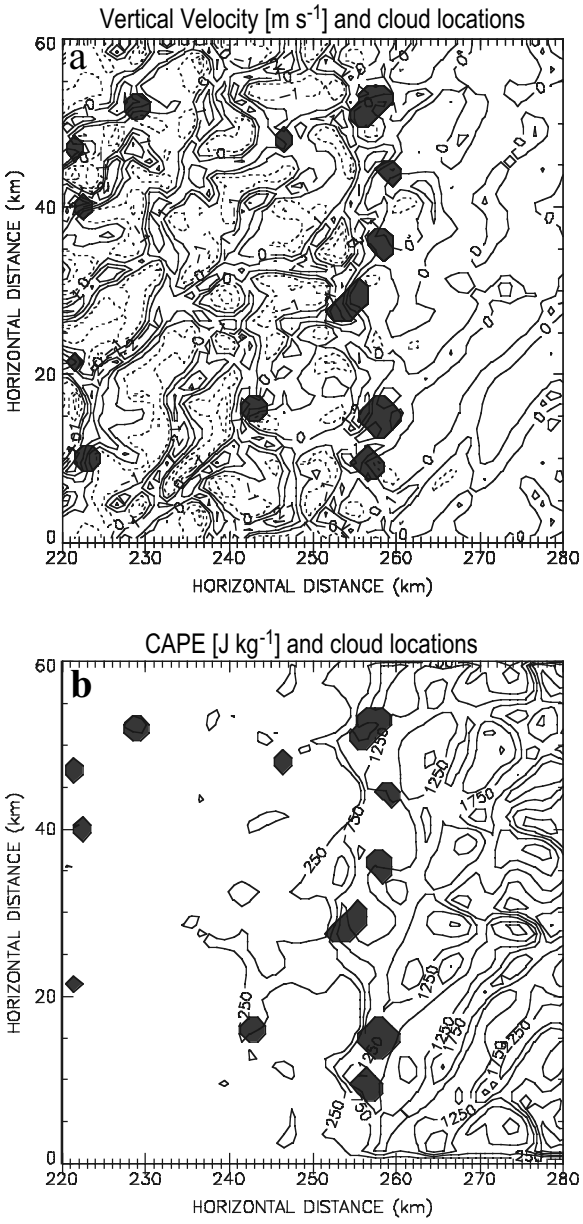

Fig. 6. a) Horizontal plot of the vertical velocity at the tenth vertical grid level (approximately 1 km MSL) and cloud locations at 8 hours, 25 minutes into the simulation. The contour interval is 1 m s^{-1} with dashed lines represent negative values. The shaded regions reveal the locations of overlying convective clouds. b) Horizontal plot of surface-based CAPE and cloud locations at 8 hours, 25 minutes into the simulation. The contour interval is every 500 J kg^{-1}. The shaded regions reveal the locations of convective clouds.

numerical simulations (Atkins et al. 1995, Dailey and Fovell 1999). The latter study identified two mechanisms that might explain the formation of the along-line undulations in the sea breeze. The first is the interaction between the HCR circulations and the boundary updraft. Along the descending branch of the HCRs the strong westerly flow transports the dryline boundary farther eastward. Conversely, along the ascending branch of the HCRs the dryline is transported westward by the stronger easterly winds within the eastern CBL. The along-line differences in wind speed combine to create the east-west undulations. The second is the convergence of moisture under the ascending branches of the HCRs. The alternating regions of increased (decreased) moisture within the CBL produce the cross-boundary shift in the sea breeze. Similar mechanisms appear to be operating within the simulated dryline environment; however, unlike the sea-breeze simulations, the simulated dryline environment also has HCRs located on the eastern side of the boundary that appear to modulate the along-line undulations via enhanced low-level easterly flow and low-level moisture convergence.

Shallow convective cloud streets develop above the HCRs starting around 4 hours into the simulation. The clouds are initially located well to the east of the developing dryline. After 6 hours into the simulation, the shallow convective clouds remain in the eastern half of the domain with cloud bases at the top of the CBL and cloud tops below 2 km MSL. In addition, around this time, as the western CBL height increases to over 4 km MSL, a few convective clouds develop in the western domain half at the top of the western CBL. These clouds tend to remain relatively shallow with elevated bases around 4 to 4.5 km MSL and tops around 5.5 to 6 km MSL.

Around 8.25 hours into the simulation, deep convective clouds begin to develop along the dryline (Fig. 6a). The base of the active dryline convective clouds are approximately 3.5 km MSL indicating that moisture from the eastern CBL is being drawn into the clouds. Surface-based CAPE values where the deep convective clouds develop are in excess of 1000 J kg^{-1} and are locally enhanced along the eastern HCR updrafts (Fig. 6b). The enhancement in the cape field along the updrafts appears to be produced by the increased low-level moisture along the HCR updrafts.

Trajectory analysis indicates that the air parcels producing the convective clouds originate from along and to the east of the dryline. The air parcels follow a path originating along an eastern boundary layer HCR updraft and proceeding into and along the ascending branch of the dryline circulation. In addition, the active convective clouds develop as a column of air parcels simultaneously reaching saturation instead of a single lifted air parcel (e.g., Ziegler et al. 1997).

4. REFERENCES

References are available at the NCSA website: http://redrock.ncsa.uiuc.edu/AOS/home_pubs.html.

5. ACKNOWLEDGMENTS

Support for this research project is provided by the National Science Foundation through grant number ATM-99866672. Computing support is provided by the National Center for Supercomputing Applications.